Article

Discovery Medicine 2026; 38(211): 2580–2592
https://doi.org/10.24976/Discov.Med.202638211.203

Urolithin A Alleviates Osteonecrosis and Is Associated With Regulation of *SIRT3* in Osteoclasts

Yi Xue[1], Donghua Fan[1], Pu Ying[1], Tong Lu[1], Yufan Ge[1], Jingliang Zhang[1], Xiaomeng Xue[2,*]

[1]Department of Orthopaedics, Changshu Hospital Affiliated to Nanjing University of Chinese Medicine, 215500 Changshu, Jiangsu, China
[2]Department of Stomatology, Xuzhou Medical University, 221004 Xuzhou, Jiangsu, China
*Correspondence: Xiaomengxue_xuzhou@126.com (Xiaomeng Xue)
Submitted: 8 June 2026 Revised: 13 July 2026 Accepted: 17 July 2026 Published: 24 August 2026

Background: Urolithin A (UA) is a safe and promising therapeutic strategy for aging-related disorders, including osteoporosis. Sirtuin 3 (*SIRT3*) has been reported as a potential modulator of bone-joint pathologies such as osteoclast activation. However, whether UA affects osteoclast activation and function through *SIRT3* remains unclear. This study aims to elucidate the mechanisms by which UA alleviates osteonecrosis.

Methods: Primary bone-marrow-derived macrophages (BMMs) were isolated from mice, treated with Macrophage Colony-Stimulating Factor (M-CSF) and Receptor Activator of Nuclear Factor-κB Ligand (RANKL). Mature osteoclasts were identified by Tartrate-Resistant Acid Phosphatase (TRAP) staining to assess differentiation. Cell viability was measured with Cell Counting Kit-8 (CCK-8) assays. The expression of osteoclast-related protein was detected by Western blot, and its mRNA level was detected by quantitative Real-Time polymerase chain reaction (qRT-PCR). The effects of UA on osteoclast mitophagy and mitochondrial respiration were assessed using Western blot and a Seahorse analyzer. Osteonecrosis of the femoral head was evaluated by hematoxylin and eosin staining (H&E), Safranin O/Fast Green, and TRAP staining. SIRT3 protein levels were assessed by Western blot.

Results: *In vitro*, UA (3 μM) significantly decreased the number of TRAP-positive osteoclasts ($p < 0.05$) and downregulated the expression of osteoclast-related genes (Acid phosphatase 5 (*Acp5*), cathepsin K (*Ctsk*), Matrix metallopeptidase 9 (*Mmp9*), Integrin subunit beta 3 (*Itgb3*), ATPase H+ transporting V0 subunit d2 (*Atp6v0d2*); $p < 0.05$). UA treatment reduced SIRT3 protein levels ($p < 0.05$), elevated ATPase inhibitory factor 1 (ATPIF1) acetylation, and suppressed receptor-mediated mitophagy markers (BCL2/adenovirus E1B interacting protein 3-like (Nix) and BCL2/adenovirus E1B 19 kDa protein-interacting protein 3 (Bnip3); $p < 0.05$) in osteoclasts, while impairing mitochondrial respiration and increasing mitochondrial ROS production. *SIRT3* overexpression partially reversed these effects. *In vivo*, UA administration attenuated cartilage thinning, trabecular collapse, and reduced TRAP-positive cells and *SIRT3*/Nuclear factor of activated T cells, cytoplasmic 1 (*NFATc1*) expression ($p < 0.05$) in a glucocorticoid-induced osteonecrosis mouse model.

Conclusion: UA effectively inhibits osteoclast activation and alleviates glucocorticoid-induced osteonecrosis, and its protective effects are associated with downregulation of *SIRT3* expression as well as the expression of mitophagy-related markers Nix and Bnip3. UA may represent a potential therapeutic candidate for osteoclast-mediated bone disorders.

Keywords: UA; SIRT3; osteoclast; osteonecrosis

Introduction

Osteonecrosis is a pathological bone lesion caused by compromised regional blood supply, characterized by osteocyte death, disruption of trabecular architecture, and eventual femoral head collapse [1,2]. Long-term or high-dose glucocorticoid administration is recognized as the principal non-traumatic risk factor for osteonecrosis of the femoral head [2]. Total hip arthroplasty remains the definitive surgical intervention for advanced osteonecrosis of the femoral head, providing pain relief and functional restoration [3]. Nevertheless, non-traumatic patients face a markedly increased risk of post-operative dislocation [4]. During the repair of osteonecrosis, aberrantly elevated osteoclast activity further undermines osseous integrity and precipitates subchondral fractures [5]. Elucidating the mechanisms governing osteoclast activation is of great value for improving the success rate of joint replacement in affected individuals.

The sirtuin family comprises NAD^+-dependent deacetylases, deacylases, and ADP-ribosyltransferases [6], which usually possess multiple functions, including metabolic control, epigenetic modification, and lifespan extension [7]. Among them, Sirtuin 1 (*SIRT1*), Sirtuin 3(*SIRT3*), Sirtuin 6 (*SIRT6*), and Sirtuin 7 (*SIRT7*) modulate bone cells to directly regulate skeletal development and homeostasis [8]. In particular, *SIRT3* drives osteoclast mitochondrial mass and promotes mitochondrial activity

and the maturation and function of osteoclasts in a PTEN-induced kinase 1 (*PINK1*)-independent manner, thereby engendering bone loss in mice [9], underscoring its crucial role in osteoclast activation. Our previous work further demonstrated that inhibiting the expression of *SIRT3* can prevent bone resorption and the generation of osteoclasts by suppressing Extracellular signal-regulated kinase (ERK) and c-Jun N-terminal kinase (JNK) signaling pathways [10]. Thus, given that excessive osteoclast formation and activation of bone resorption are recognized drivers of widespread bone destruction and implant failure [11], identifying a gene or drug that effectively targets *SIRT3* to counter osteoclastogenesis may represent a promising therapeutic strategy for improving osteonecrosis outcomes.

Urolithin A (UA), a natural metabolite generated by gut microbiota from dietary ellagitannins and ellagic acid, has antioxidant, anti-inflammatory, anti-apoptotic, and anti-carcinogenic properties, offering protection against neurodegeneration and aging-related disorders that affect muscle, brain, joints, and other organs [12,13,14,15]. Additionally, UA confers beneficial effects against joint structural damage by attenuating cartilage degeneration, an action mediated through the modulation of mitochondrial function [16]. Notably, emerging evidence implicates UA in modulating osteoclast activity. For instance, UA can inhibit Receptor Activator of Nuclear Factor-κB Ligand (RANKL) -induced osteoclastogenesis and post-menopausal osteoporosis by suppressing inflammation and the pyroptosis pathway activated by downstream Nuclear factor-κB (NF-κB) [17]. A prior study further report that UA can regulate the sirtuin family member *SIRT1* [18]. However, whether UA influences osteoclast activation via other sirtuins, such as *SIRT3*, and the role it plays in the treatment of osteonecrosis has not yet been systematically studied.

The present study investigated the impact of UA on osteoclast activation and osteonecrosis. We hypothesized that the protective effect of UA against osteonecrosis is closely attributed to the downregulation of *SIRT3* expression and the subsequent inhibition of aberrant osteoclast activity. Using *in vitro* assays and *in vivo* models, we evaluated the effects of UA on *SIRT3* expression and its consequent regulation of osteoclast activation and function. This study aimed to elucidate whether UA regulates osteoclast activation and function through *SIRT3*, and to evaluate its therapeutic potential in a mouse model of glucocorticoid-induced osteonecrosis.

Materials and Methods

Mouse Experiments

All animal procedures were approved by the Animal Research Ethics Committee of Changshu Hospital Affiliated to Nanjing University of Chinese Medicine (approval date: September 5, 2025), and conducted in strict accordance with the Guide for the Care and Use of Laboratory Animals (8th ed., National Academies Press, 2011) and the ARRIVE Guidelines 2.0.

C57BL/6 mice (8-week-old, 20–25 g, male) were randomly assigned to three groups: Sham, Model, and Model+UA, using a computer-generated random number table with 8 mice per group (n = 8/ group). Mice in the Model and Model+UA groups received two intraperitoneal injections of lipopolysaccharide (LPS, HY-D1056, MCE, Princeton, NJ, USA) at 20 μg/kg (injection volume: 100 μL), with a 24 h interval. Mice were subsequently given intramuscular injections of methylprednisolone sodium succinate (HY-B1900, MCE, Princeton, NJ, USA) at 40 mg/kg (injection volume: 100 μL), 4 times per week with intervals of 24 h. Sham mice received sterile saline solution of equivalent volumes (100 μL) with the same frequencies and durations. In addition, the Model+UA group received daily intraperitoneal injections of UA (HY-100599, MCE, Princeton, NJ, USA) at 50 mg/kg (dissolved in 2% Dimethyl sulfoxide (DMSO) + 98% sterile saline, injection volume: 100 μL), whereas the other groups received equivalent volumes of the vehicle (2% DMSO + 98% sterile saline). The administration period was completed for 4 weeks. All animals were housed under standard conditions (12 h light/dark cycle, 22 ± 2 °C, 50 ± 10% humidity) with free access to food and water. During tissue harvesting and subsequent histological analyses, the investigators were blinded to the group assignments. After 4 weeks, animals were euthanized by cervical dislocation under deep anesthesia induced by intraperitoneal injection of pentobarbital sodium (50 mg/kg), and femoral heads were carefully harvested for use. Eight mice per group were used for model establishment. For histological and molecular analyses, three mice were randomly selected from each group for further examination.

Cell Selection and Culture

Since macrophages are the principal producers of pro-inflammatory cytokines elicited by wear debris during osteolysis, primary bone-marrow-derived macrophages (BMMs) were obtained from the bone marrow flushed from femora and tibiae of 6-week-old female C57BL/6 mice (Model Organisms Center, Shanghai, China). Cells were cultured in α-MEM supplemented with 10% fetal bovine serum (FBS) and 1% penicillin-streptomycin at 37 °C under 5% CO_2. Non-adherent cells were removed, and the remaining cells were seeded in 24-well plates and stimulated with Macrophage Colony-Stimulating Factor (M-CSF) plus RANKL to induce macrophage differentiation towards osteoclasts. BMMs were stimulated with M-CSF (30 ng/mL) plus RANKL (50 ng/mL) in the presence or absence of UA to induce differentiation towards osteoclasts [10]. After 6 days, mature osteoclasts (≥3 nuclei) were identified by Tartrate-Resistant Acid Phosphatase (TRAP) staining (see Section *TRAP Staining*) and used for subsequent assays. Mycoplasma contamination was routinely monitored using a Mycoplasma Detection Kit (Beyotime, Shanghai, China)

Table 1. qRT-PCR primers.

Primer	Forward (5′-3′)	Reverse (5′-3′)
Sirtuin 3 (*SIRT3*)	CGGCTCTATACACAGAACATCG	CATCAGCCCATATGTCTTCCC
Acid phosphatase 5 (*Acp5*)	ACATGACCACAACCTGCAG	CCTCAGATCCATAGTGAAACCG
Cathepsin K (*Ctsk*)	TGACCACTGCCTTCCAATAC	CTCTGTACCCTCTGCATTTAGC
Matrix metallopeptidase 9 (*Mmp9*)	GATCCCCAGAGCGTCATTC	CCACCTTGTTCACCTCATTTTG
Integrin subunit beta 3 (*Itgb3*)	TCGTCAGCCTTTACCAGAATT	CGTACTTCCAGCTCCACTTTAG
ATPase H+ transporting V0 subunit d2 (*Atp6v0d2*)	CTAGTGCAGTGTGAGACCTTG	TTAGCCAGGAAGTTGCCATAG
β-actin	ACCTTCTACAATGAGCTGCG	CCTGGATAGCAACGTACATGG

according to the manufacturer's instructions. All cell cultures were confirmed to be mycoplasma-free prior to experiments. The working concentration of UA in subsequent experiments was 3 μM.

Cell Transfection

Plasmids encoding *SIRT3*-overexpression (oe-*SIRT3*) and negative control (oe-NC) were designed and synthesized by GenePharma (Shanghai, China). The oe-*SIRT3* plasmid was constructed by cloning the full-length coding sequence of mouse *SIRT3* (NCBI RefSeq: NM_001017524.3) into the pcDNA3.1(+) vector. The constructed plasmid was verified by Sanger sequencing (performed by GenePharma) to confirm the correct insertion and sequence integrity. Subsequently, the aforementioned plasmids were transfected into BMMs using Lipofectamine 2000 (11668500, Invitrogen, Waltham, MA, USA), with detailed conditions described as follows: BMMs were seeded in 24-well plates at a density of 2×10^5 cells per well 24 h prior to transfection to reach 70%–80% confluence at transfection. A total of 2 μg plasmid DNA and 5 μL Lipofectamine 2000 were added to each well. After 6 h of incubation, the medium was replaced with complete medium supplemented with M-CSF and RANKL for subsequent culture. Transfection efficiency was verified by detecting SIRT3 protein expression via western blot (WB).

quantitative Real-Time polymerase chain reaction (qRT-PCR)

qRT-PCR was employed to quantify the expression of osteoclast-related genes during osteoclast differentiation. Briefly, total RNA was extracted with TRIzol (R0016, Beyotime, Shanghai, China) and reverse-transcribed into cDNA using PrimeScript RT reagent (RR037A, Kusatsu, Takara, Japan). SYBR Premix Ex Taq (RR420A, Kusatsu, Takara, Japan) was used to prepare qRT-PCR and monitor amplification of DNA during PCR in real time. Target gene expression was detected on an ABI 7900 HT Real-Time PCR System (Applied Biosystems, Waltham, MA, USA). *β-actin* served as the internal reference, and all reactions were run in triplicate. Relative gene expression was calculated using the $2^{-\Delta\Delta Ct}$ method. Primer sequences are listed in Table 1.

WB

Proteins were extracted from cell and tissue samples with Radioimmunoprecipitation assay (RIPA) lysis buffer (R0278, Sigma-Aldrich, St. Louis, MO, USA) and centrifuged at 12000 rpm. Proteins were then collected from the supernatants, and concentrations were determined using BCA protein assay kits (23225, Thermo Fisher Scientific, Waltham, MA, USA). Proteins were separated on 10% Sodium dodecyl sulfate-polyacrylamide gel electrophoresis (SDS-PAGE) and transferred to Polyvinylidene fluoride (PVDF) membranes. Membranes were blocked with QuickBlock™ blocking buffer (P0252, Beyotime, Shanghai, China) to reduce non-specific binding, then incubated overnight at 4 °C on a shaker with the following primary antibodies from Abcam (Cambridge, UK): Rabbit anti-SIRT3 (ab246522, diluted at 1:1000), Rabbit anti-Nuclear factor of activated T cells, cytoplasmic 1 (NFATc1) (ab25916, diluted at 1:1000), Rabbit anti-BCL2/adenovirus E1B interacting protein 3-like (Nix) (ab155010, diluted at 1:1000), Rabbit anti-BCL2/adenovirus E1B 19 kDa protein-interacting protein 3 (Bnip3) (ab109362, diluted at 1:1000), and Rabbit anti-β-actin (ab8227, diluted at 1:5000). After washing, membranes were incubated with HRP-conjugated Goat anti-Rabbit IgG (ab6721, Abcam, Cambridge, UK, diluted at 1:5000). Signals were visualized using BeyoECL Plus (Beyotime, Shanghai, China), an ultrasensitive Enhanced chemiluminescence (ECL) chemiluminescence kit (PK10003, Proteintech, Wuhan, China), and were quantified with ImageJ 6.0 software (NIH, Bethesda, MD, USA).

Acetylation Assay

To assess the acetylation level of ATPase inhibitory factor 1 (ATPIF1), cell lysates were centrifuged at 12000 ×g for 15 min at 4 °C, and the resulting supernatants were collected. Protein concentrations were determined using the BCA method (Thermo Fisher Scientific, Waltham, MA, USA). A total of 500 μg of protein was incubated with an anti-ATPIF1 antibody (#8528, Cell Signaling, USA, diluted at 1:100) for 2 h at 4 °C, followed by an additional 1 h incubation with Protein A/G magnetic beads. After thorough washing, the immune complexes were eluted by boiling. The eluted samples were resolved by 10% SDS-PAGE and transferred onto membranes. The membranes were then

incubated overnight at 4 °C with an anti-acetylated-lysine antibody (#9441, Cell Signaling, USA, diluted at 1:1000), followed by a 1 h incubation at room temperature with an HRP-conjugated goat anti-rabbit IgG secondary antibody (ab6721, Abcam, Cambridge, UK, diluted at 1:5000). Finally, chemiluminescent detection was performed using the BeyoECL Plus (Ultra-sensitive ECL Chemiluminescence Kit; Beyotime, Shanghai, China). Band gray-scale analysis of AC-Lys was performed using ImageJ 6.0 software.

Mitochondrial Respiration

BMMs were seeded into Seahorse XF96 microplates (102416, Agilent, Santa Clara, CA, USA) at a density of 1.5×10^4 cells per well. Subsequently, osteoclast differentiation was induced by M-CSF and RANKL in the presence or absence of 3 μM UA. Upon completion of differentiation, the culture medium was discarded and replaced with XF assay medium (103575, Agilent, Santa Clara, CA, USA). The culture plates were then equilibrated in a CO_2-free incubator at 37 °C for 20 min. Basal respiration levels were recorded three times using an XF96 analyzer. Subsequently, 10 μg/mL oligomycin (495455, Sigma-Aldrich, St. Louis, MO, USA) was added to inhibit mitochondrial ATP synthase, and the decline in oxygen consumption rate (OCR) corresponding to ATP turnover was measured. Next, 5 μM of the oxidative phosphorylation uncoupler FCCP (C2920, Sigma-Aldrich, St. Louis, MO, USA) was injected to determine maximal respiratory capacity. A mixture of 10 μM antimycin A (77332, Sigma-Aldrich, St. Louis, MO, USA) and 10 μM rotenone (R8875, Sigma-Aldrich, St. Louis, MO, USA) was added to block electron transport chain activity, allowing assessment of non-mitochondrial oxygen consumption. Parameters such as basal mitochondrial respiration and ATP-linked respiration were calculated from the obtained data according to a previously described method [9]. All acquired OCR data were normalized to the total cell count of each well.

Mitochondrial Superoxide Production

Mitochondrial superoxide levels were measured using MitoSOX Red (M36008, Thermo Fisher Scientific, Waltham, MA, USA), a mitochondria-specific probe. Cells were seeded in black 96-well microplates. After treatment with 3 μM UA, the medium was replaced with assay medium containing 3 μM MitoSOX, followed by a 30 min incubation at 37 °C. Kinetic measurements were then performed over 120 min using a Cytation™ 5 multimode plate reader (BioTek, Winooski, VT, USA). The oxidation rate of MitoSOX was evaluated by monitoring fluorescence signals at $\lambda_{ex}/\lambda_{em}$ = 510/580 nm.

Cell Counting Kit-8 (CCK-8) Cell Viability Assay

A CCK-8 kit (C0038, Beyotime, Shanghai, China) was used to assess the cytotoxicity of UA toward BMMs. BMMs were seeded at 5000 cells per well in 96-well plates, treated with UAat concentrations of 0, 1, 2, 3, 4, 5, and 6 μM, and incubated in an Vios™ iDx 255 L CO2 Incubators (Thermo Fisher Scientific, Waltham, MA, USA) for 24 h or 48 h at 37 °C with 5% CO_2. 10 μL of CCK-8 reagent was added to each well and incubated for 2 h. Absorbance (OD value) at 450 nm was measured with a Varioskan LUX multimode microplate reader (Thermo Fisher Scientific, Waltham, MA, USA) to determine optimal concentration and time of UA treatment.

To evaluate the effect of long-term UA treatment on BMMs viability, cells were seeded in 96-well plates at a density of 5×10^3 cells per well and cultured in complete medium containing M-CSF (30 ng/mL) and RANKL (50 ng/mL). Fresh medium supplemented with 3 μM UA was replaced daily over a continuous 6-day culture period, with complete medium containing UA being renewed every 2 days. After 6 days, the original medium was discarded, and 100 μL of fresh medium containing 10 μL of CCK-8 reagent was added to each well, followed by incubation at 37 °C for 2 h. The OD was then measured at 450 nm.

TRAP Staining

BMMs were seeded at 8×10^4 cells per well in 24-well plates and stimulated with RANKL and M-CSF in the presence or absence of UA to induce osteoclast differentiation. Femurs were decalcified with Ethylenediaminetetraacetic acid (EDTA) solution (1.08431, Sigma-Aldrich, St. Louis, MO, USA) for 28 days, embedded in paraffin, and sectioned with a paraffin microtome (Leica, Germany). A TRAP staining kit (387A, Sigma-Aldrich, St. Louis, MO, USA) was then used to assess osteoclast differentiation in cells or tissue sections. After staining, samples were examined under a high-resolution microscope (Axio Imager 2, Zeiss, Oberkochen, Germany). In *in vitro* experiments, ImageJ 6.0 software was applied to count TRAP-positive multinucleated cells (≥3 nuclei per cell). For *in vivo* bone tissue sections, accurate enumeration of multinucleated cells was unfeasible, as osteoclasts adhered to bone surfaces and frequently exhibited distorted incomplete morphology due to compression by the bone matrix. Accordingly, the percentage of TRAP-positive area (TRAP-positive area / total bone tissue area × 100%) was adopted as the quantitative indicator, and ImageJ 6.0 software was utilized to measure the area of positive signals.

Hematoxylin and eosin staining (H&E) Staining

H&E staining kits (C0105, Beyotime, Shanghai, China) were employed for histological assessment. Paraffin-embedded femoral sections were deparaffinized with xylene and rehydrated through graded ethanol: absolute ethanol for 5 min, followed by 2 min each in 90%, 80%, and 70% ethanol, and a final rinse in distilled water for 2 min. Sections were stained with hematoxylin for 10 min, rinsed, then counterstained with eosin for 1 min. After dehydration, clearing, and mounting, sections

were examined under a Zeiss microscope (Axio Imager 2, Oberkochen, Germany). Nuclei appeared blue and cytoplasm pink or red.

The Osteoarthritis Research Society International (OARSI) grading system was applied to evaluate cartilage degeneration in femoral head sections. Scores were assigned based on the extent of cartilage surface degeneration and structural changes, ranging from grade 0 (normal) to grade 6 (severe degeneration). In this study, the OARSI score only acted as an auxiliary reference for evaluating cartilage degeneration rather than the primary criterion for judging the severity of osteonecrosis [19,20]. The severity of osteonecrosis was assessed using more specific histological markers, including empty lacunae and trabecular collapse. Two independent observers blinded to the treatment groups performed the scoring.

Safranin O/Fast Green Staining

Femoral heads were fixed in 10% paraformaldehyde, decalcified, paraffin-embedded, and serially sectioned. Sections were stained with Weigert's hematoxylin (HT1079, Sigma-Aldrich, St. Louis, MO, USA) for 10 min, washed in running water, then counterstained with fast green (Solarbio, China) for 6 min and differentiated in 1% acetic acid for 30 s. Subsequently, sections were stained with 0.1% safranin O (S2255, Sigma-Aldrich, St. Louis, MO, USA) for 12 min, rinsed with deionized water, differentiated in 70% ethanol, dehydrated, and mounted with Eukitt (03989, Sigma-Aldrich, St. Louis, MO, USA). Images were captured under a Zeiss microscope (Axio Imager 2, Oberkochen, Germany).

Immunohistochemistry (IHC) Staining

Paraffin-embedded femoral sections were baked at 60 °C for 30 min, deparaffinized in xylene, and rehydrated through a graded ethanol series. Antigen retrieval was performed by heating the sections in 0.01 M sodium citrate buffer at 95 °C for 20 min. Endogenous peroxidase activity was blocked with 3% H_2O_2 for 15 min at room temperature, followed by incubation with 5% bovine serum albumin (BSA) (MCE, Monmouth Junction, NJ, USA) for 30 min at 37 °C to block nonspecific binding. The sections were then incubated overnight at 4 °C with a rabbit anti-SIRT3 antibody (CST #5490, Cell Signaling, Danvers, MA, USA, diluted at 1:200). After washing with PBS, a horseradish peroxidase (HRP)-conjugated goat anti-rabbit IgG secondary antibody (SAB3700885, Sigma, St. Louis, MO, USA, diluted at 1:5000) was applied for 30 min at 37 °C. Subsequently, 3,3'-diaminobenzidine (DAB) (HY-W025920, MCE, Monmouth Junction, NJ, USA) chromogen solution was added, and the reaction was terminated once a distinct brick-red color developed. Finally, the nuclei were counterstained with hematoxylin, and the sections were mounted with a mounting medium prior to microscopic observation. Five random high-power fields (×200 magnification) were captured per section and analyzed using ImageJ 6.0 software. The percentage of SIRT3-positive area was calculated as: total area of SIRT3-positive cells / total tissue area within each field × 100%.

Immunofluorescence (IF) Staining

Following the same deparaffinization and antigen retrieval procedure described above, sections were permeabilized with 0.3% Triton X-100 (9002-93-1, Solarbio, Beijing, China) for 15 min and blocked with 5% BSA for 30 min. The sections were then incubated overnight at 4 °C with a rabbit anti-NFATc1 antibody (ab25916, Abcam, Cambridge, UK, diluted at 1:100). After washing with PBS, an Alexa Fluor 488-conjugated goat anti-rabbit IgG secondary antibody (ab150077, Abcam, Cambridge, UK, diluted at 1:500) was applied for 1 h at 37 °C. Nuclei were counterstained with 4',6-diamidino-2-phenylindole(DAPI) (HY-D2868, MCE, Monmouth Junction, NJ, USA) for 5 min. The sections were mounted with an antifade mounting medium and visualized under a fluorescence microscope (Axio Imager 2, Zeiss, Oberkochen, Germany). Five random high-power fields (×200 magnification) were selected from each section. The average fluorescence intensity of NFATc1 green fluorescence was quantified using ImageJ 6.0 software, defined as the mean fluorescence intensity of NFATc1 signals covering all DAPI-positive regions within each field. Sections from at least three animals were analyzed per group. Additionally, the proportion of nuclear NFATc1-positive cells was quantified, calculated as the percentage of cells with colocalized NFATc1 green fluorescence and DAPI blue signals relative to the total number of DAPI-positive cells. No fewer than 500 cells were counted for each group.

Statistical Analysis

All data were analyzed using GraphPad Prism 8.0 (GraphPad, San Diego, CA, USA) and are expressed as mean ± standard deviation. All quantitative data were first assessed for normality using the Shapiro–Wilk test. Data conforming to a normal distribution ($p > 0.05$) were subsequently analyzed using parametric tests. Comparisons between two groups were performed with unpaired *t*-tests. Multiple-group comparisons were made using one-way ANOVA followed by Tukey's post hoc test for multiple comparisons. All stained images were independently reviewed in a blinded manner by a pathologist to confirm that intergroup differences observed in the images were consistent with the descriptions in the manuscript. $p < 0.05$ was considered statistically significant.

Results

In Vitro Investigation of the Effects of UA on Osteoclast Activation and Function

First, we examined the influence of various concentrations of UA (MCE, USA) on the viability of mouse BMMs cultured for 24 h or 48 h. As shown in Fig. 1A, 24 h of UA treatment did not significantly affect BMM viability. Influence on cell viability after UA treatment at ≤3 μM for 48 h remained non-significant. Furthermore, compared with the control group, treatment with 3 μM urolithin A for 6 days had no significant effect on BMMs cell viability (Fig. 1A). Based on these results, all subsequent *in vitro* experiments were performed with continuous UA intervention at 3 μM, starting from Day 0 of differentiation induction, with fresh UA supplemented daily upon medium replacement until the respective experimental endpoints. In this study, BMMs were further stimulated with M-CSF (30 ng/mL) and RANKL (50 ng/mL) for 6 days. TRAP staining revealed abundant multinucleated (≥3 nuclei) TRAP-positive cells (Fig. 1B). WB analysis demonstrated markedly elevated protein levels of NFATc1, a master transcription factor governing osteoclastogenesis (Fig. 1C). qRT-PCR results exhibited significant upregulation of osteoclast-specific marker genes including *Acp5*, *Ctsk*, *Mmp9*, *Itgb3*, and *Atp6v0d2* (Fig. 1D). Collectively, these data confirm the successful differentiation of BMMs into mature osteoclasts.

BMMs were subsequently stimulated with or without UA treatment during osteoclast differentiation induced by RANKL and M-CSF, to evaluate the effects of UA on osteoclast activation and function. TRAP staining results revealed that the number of TRAP-positive osteoclasts was markedly reduced in the UA-treated group ($p < 0.05$) (Fig. 1B), indicating that UA effectively inhibited osteoclastogenesis. WB analysis further demonstrated that UA treatment significantly downregulated the protein level of NFATc1 ($p < 0.05$) (Fig. 1C). qRT-PCR assays showed that the mRNA expression of *Acp5*, *Ctsk*, *Mmp9*, *Itgb3*, and *Atp6v0d2*, was substantially decreased following UA intervention ($p < 0.05$) (Fig. 1D). To rule out the possibility that the reduction in TRAP-positive cells resulted from long-term cytotoxicity of UA, we further detected cell viability after continuous treatment with 3 μM UA for 6 days. CCK-8 assay results showed that 3 μM UA treatment exerted no significant effect on BMMs cell viability compared with the control group (Fig. 1A), confirming that this concentration of UA exhibits no obvious long-term cytotoxicity within the experimental period. Collectively, these data demonstrated that UA inhibited osteoclast activation and function.

UA Regulates Osteoclast Activation and Mitochondrial Function by Modulating SIRT3 Expression

Given the pronounced effects of UA on osteoclast activation and function, we next explored whether these effects were mediated by *SIRT3*. During the course of continuous UA intervention, SIRT3 protein levels were examined on Days 1, 3, and 5. WB revealed that SIRT3 levels were significantly lower in the UA-treated groups than in the corresponding control groups at each time point. Moreover, SIRT3 protein expression in osteoclasts exhibited a progressive decline with increasing duration of UA treatment ($p < 0.05$) (Fig. 2A). A previous study has shown that *SIRT3* promotes receptor-mediated mitophagy in osteoclasts by deacetylating *ATPIF1*, thereby facilitating osteoclast maturation and function [9]. Based on these findings, we hypothesized that UA enhances ATPIF1 acetylation by reducing *SIRT3* levels, consequently affecting mitophagy and osteoclast maturation. To test this hypothesis, BMMs treated with UA were additionally transfected with a *SIRT3* overexpression vector (oe-*SIRT3*). WB analysis revealed that UA treatment led to a marked decrease in SIRT3 protein levels, whereas oe-*SIRT3* transfection substantially restored *SIRT3* expression, further corroborating the inhibitory effect of UA on *SIRT3*. Quantitative analysis revealed that oe-*SIRT3* transfection increased SIRT3 protein levels by approximately 1.8-fold compared with the oe-NC group ($p < 0.05$), confirming the successful overexpression of *SIRT3* in BMMs ($p < 0.05$) (Fig. 2B). Examination of mitophagy-related proteins showed that UA treatment significantly reduced the protein levels of Nix and Bnip3, two markers of receptor-mediated mitophagy; this reduction was partially reversed upon *SIRT3* overexpression ($p < 0.05$) (Fig. 2B). Acetylation analysis demonstrated that UA treatment affected the acetylation level of ATPIF1, while *SIRT3* overexpression reduced the Ac-lys level (Fig. 2B). Notably, UA treatment also markedly suppressed both basal mitochondrial respiration and ATP-linked respiration in BMMs ($p < 0.05$) (Fig. 2C), accompanied by a pronounced increase in mitochondrial reactive oxygen species levels ($p < 0.05$) (Fig. 2D). Collectively, these results suggested that UA, by downregulating *SIRT3* expression, and then maybe enhance ATPIF1 acetylation, thereby impairing mitophagic capacity and compromising mitochondrial function in osteoclasts. Furthermore, TRAP staining revealed that UA treatment significantly inhibited osteoclast formation, and this inhibitory effect on osteoclast differentiation and activation was notably reversed by *SIRT3* overexpression ($p < 0.05$) (Fig. 2E). Taken together, these findings suggested that *SIRT3* plays an important role in mediating the effects of UA on mitophagy and differentiation in osteoclasts, though additional mechanisms may also contribute. The overexpression rescue experiments provide evidence that restoring *SIRT3* levels can partially reverse UA's inhibitory effects, supporting the involvement of *SIRT3* in UA's mechanism of action.

UA Alleviates Osteonecrosis of the Femoral Head

Given that our earlier *in vitro* data demonstrated that UA effectively suppressed osteoclastogenesis, we next

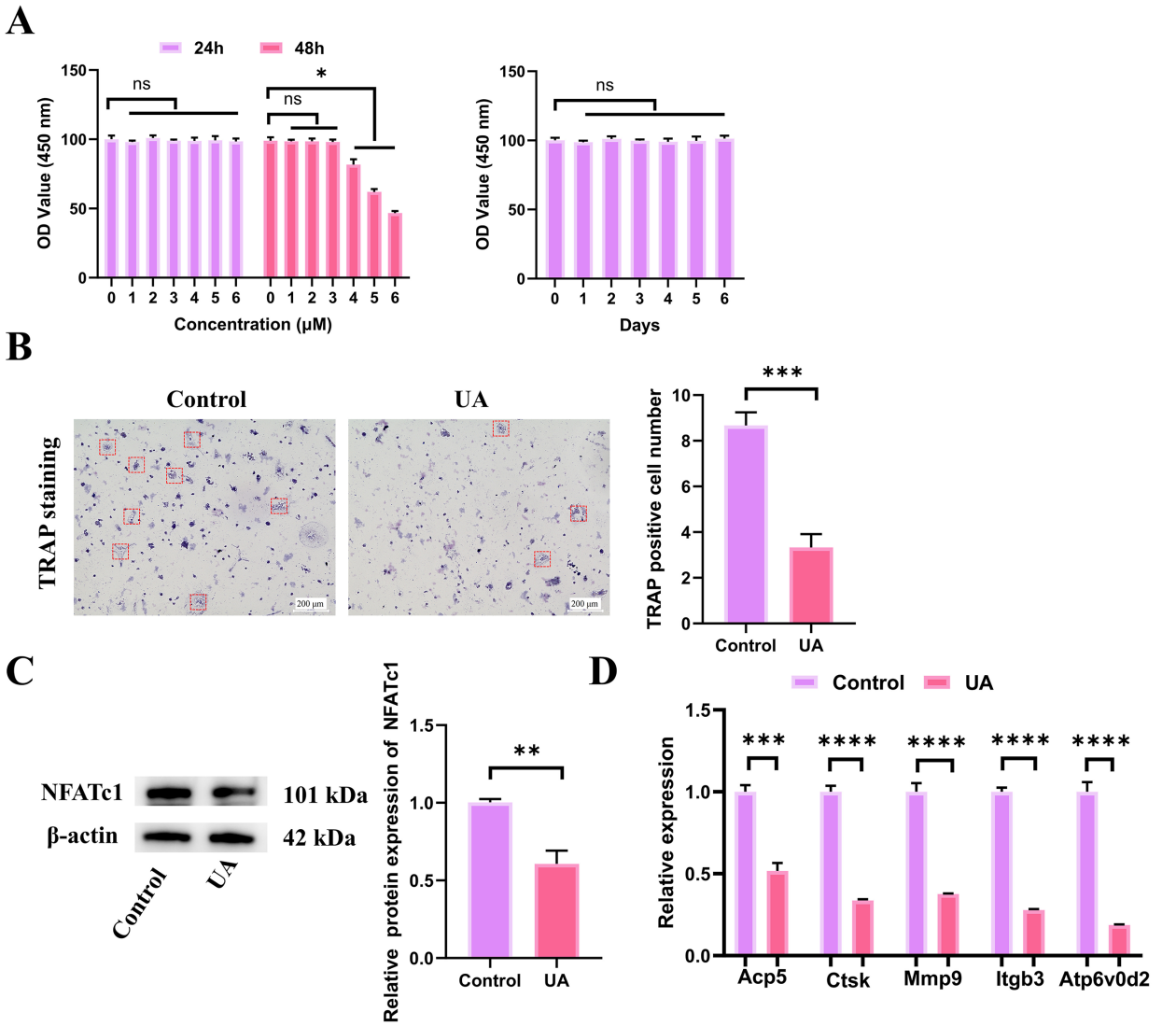

Fig. 1. Effects of UA on osteoclast activation and function *in vitro*. BMMs were stimulated with M-CSF and RANKL in the presence or absence of UA to induce osteoclast differentiation: (A) The effects of 0, 1, 2, 3, 4, 5, and 6 μM UA on cell viability were detected at 24 h and 48 h after treatment (left panel) (n = 3). The cell viability was further examined by CCK-8 assay following continuous treatment with 3 μM UA for 6 days (right panel) (n = 3). (B) Representative images of TRAP staining and quantitative analysis of TRAP-positive cells (n = 3). The red boxes indicate TRAP-positive multinucleated osteoclasts. (C) WB analysis and quantitative quantification of the protein expression of NFATc1, a key osteoclast marker (n = 3); (D) qRT-PCR quantification of mRNA levels of osteoclast differentiation- and function-related genes (*Acp5*, *Ctsk*, *Mmp9*, *Itgb3*, and *Atp6v0d2*) (n = 3). $*p < 0.05$, $**p < 0.01$, $***p < 0.001$, $****p < 0.0001$, ns, not significant. All n = 3 refer to three independent biological replicates. UA, Urolithin A; BMMs, bone-marrow-derived macrophages; M-CSF, Macrophage Colony-Stimulating Factor; RANKL, Receptor activator of nuclear factor-κB ligand; CCK-8, Cell Counting Kit-8; TRAP, Tartrate-resistant acid phosphatase; WB, Western blot; NFATc1, Nuclear factor of activated T cells, cytoplasmic 1; qRT-PCR, quantitative Real-Time polymerase chain reaction; *Acp5*, Acid phosphatase 5; *Ctsk*, Cathepsin K; *Mmp9*, Matrix metallopeptidase 9; *Itgb3*, Integrin subunit beta 3; *Atp6v0d2*, ATPase H+ transporting V0 subunit d2.

constructed a murine model of glucocorticoid-related osteonecrosis of the femoral head to validate UA's role in alleviating osteonecrosis. H&E staining revealed severe structural abnormalities in the femur of the model group. Partial bone architecture was completely destroyed and replaced by hyperplastic synovial tissue with obvious fibrosis and inflammatory cell infiltration (red arrows). Fractured trabeculae with irregular margins were also observed (black arrows). In contrast, UA treatment only induced mild femoral structural defects. Focal incomplete bone tissue filled with fibrotic hyperplastic synovium and inflammatory infiltration was still present (red arrows), while the

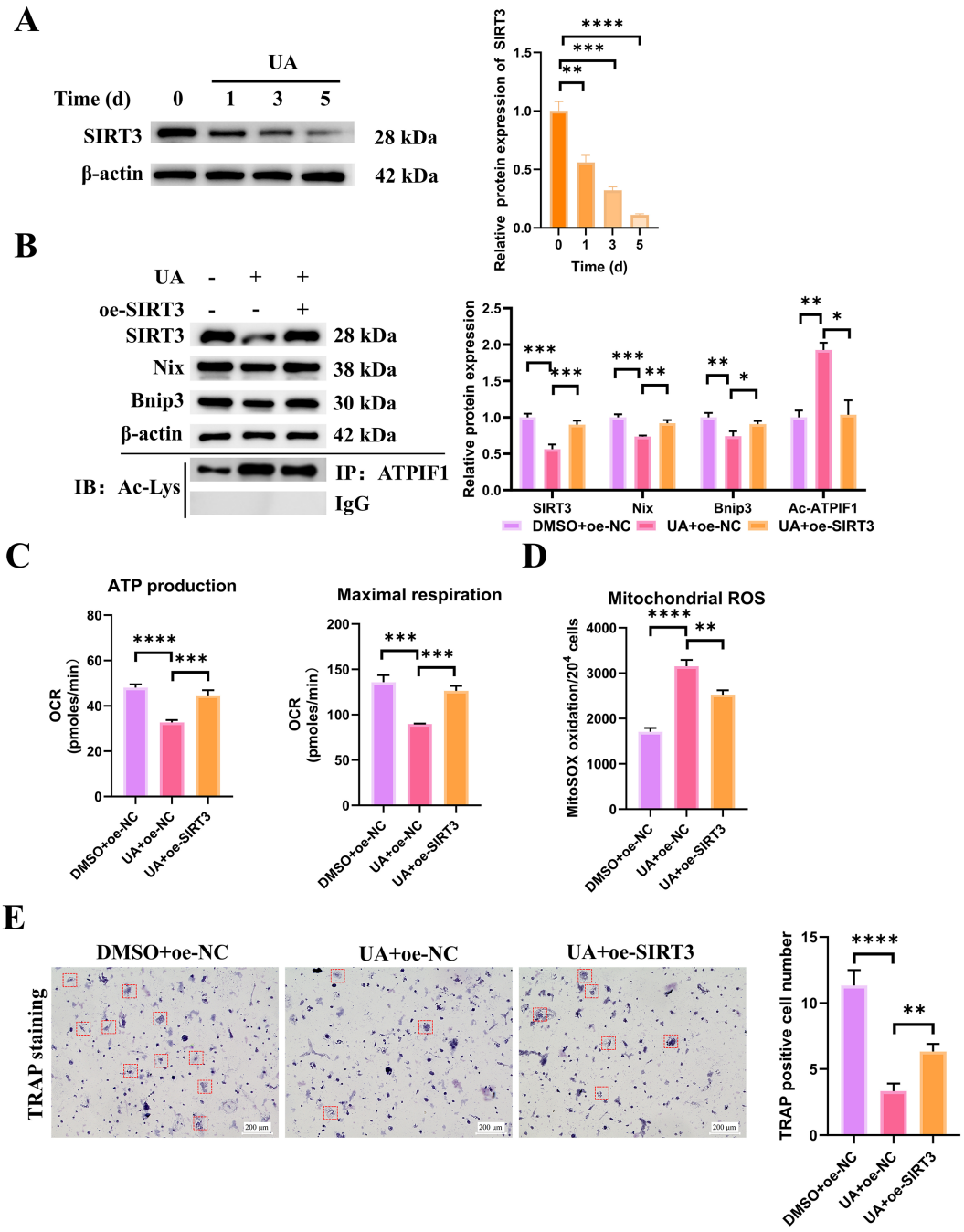

Fig. 2. UA inhibits osteoclast differentiation, mitophagy, and mitochondrial function through downregulation of *SIRT3*. During the course of continuous UA intervention, (A) WB detection and quantitative statistics of SIRT3 protein expression in osteoclasts after UA treatment for different durations (0, 1, 3, 5 days) (n = 3). (B) Protein expression levels of SIRT3, Nix, and Bnip3, along with the acetylation status of ATPIF1, were assessed in different treatment groups using WB and co-immunoprecipitation-based acetylation assays (n = 3). (C) Mitochondrial respiration and ATP-linked oxygen consumption rates were measured using a Seahorse analyzer (n = 3). (D) Mitochondrial reactive oxygen species production was evaluated with MitoSOX staining (n = 3). (E) Osteoclast differentiation under various treatment conditions was analyzed by TRAP staining (n = 3), red boxes in the figure mark TRAP-positive multinucleated osteoclasts. *$p < 0.05$, **$p < 0.01$, ***$p < 0.001$, ****$p < 0.0001$. DMSO, Dimethyl sulfoxide; *SIRT3*, Sirtuin 3; Nix, BCL2/adenovirus E1B interacting protein 3-like; Bnip3, BCL2/adenovirus E1B 19 kDa protein-interacting protein 3; IB, Immunoblotting; IP, Immunoprecipitation; ATPIF1, ATPase inhibitory factor 1; OCR, oxygen consumption rate.

medullary cavity exhibited compact bone marrow and intact trabeculae without thinning (Fig. 3A). Safranin O/Fast Green staining showed smooth and intact articular cartilage surfaces with uniformly red-stained cartilage matrix and normal cartilage thickness in the sham group. The model group displayed abundant blue-green fibrous tissue at bone defect sites with negligible cartilage formation. After UA intervention, the area of red cartilage matrix was markedly expanded and cartilage architecture was partially restored (Fig. 3A). Consistently, the model group had significantly higher OARSI scores relative to the sham group, whereas UA administration markedly reversed this elevation ($p < 0.05$) (Fig. 3E). TRAP staining demonstrated abundant TRAP-positive osteoclasts (wine-red cytoplasm, pale blue nuclei) lining bone surfaces in the model group. Compared with the model group, the TRAP-positive staining area was significantly reduced in the UA treatment groups ($p < 0.05$) (Fig. 3B,F). Further IHC and IF analyses were performed to assess the expression of SIRT3 and NFATc1 in femoral tissues. Compared with the Sham group, the Model group exhibited markedly elevated levels of both SIRT3 and NFATc1, whereas UA administration significantly reduced their expression ($p < 0.05$) (Fig. 3C,D,G,H). WB analysis yielded consistent results, confirming that UA downregulated SIRT3 and NFATc1 protein levels in mouse femurs ($p < 0.05$) (Fig. 3I). Concomitantly, relative to the control group, the Model group showed pronounced increases in the protein levels of the receptor-associated mitophagy markers Nix and Bnip3, which were attenuated following UA treatment ($p < 0.05$) (Fig. 3I). Taken together, the present findings demonstrated that UA effectively alleviated osteonecrosis in mice, and this protective effect was closely associated with *SIRT3*-dependent regulation of mitophagy.

Discussion

Total hip arthroplasty, the primary treatment for osteonecrosis of the femoral head, has shown variable long-term outcomes, with younger patients facing particular challenges including implant longevity and post-operative complications [4,21]. Restoration of the femoral head relies on a delicate equilibrium between osteoblasts and osteoclasts, and inhibition of osteoclast differentiation can effectively decelerate osteonecrosis progression [5,22]. Through literature review we identified UA as a promising modulator of skeletal architecture, although the underlying mechanisms were still incompletely understood. Therefore, this study investigated the precise mechanisms by which UA regulated osteoclast activation and osteonecrosis, with a particular focus on the *SIRT3*-mediated mitophagy pathway.

Intestinal metabolite UA has been shown to suppress osteoclastogenesis and aging-related osteoporosis by enhancing autophagy in BMMs [23]. UA suppresses RANKL-induced osteoclast differentiation in a Bone morphogenetic protein 2 (BMP-2)-dependent manner [24]. Our findings corroborated these observations. A series of staining assays revealed that an optimal concentration of UA greatly reduced TRAP-positive areas and suppressed bone resorption. Consistently, qRT-PCR showed that UA downregulated the expression of key osteoclastic genes (*Acp5*, *Ctsk*, *Mmp9*, *Itgb3*, and *Atp6v0d2*), confirming its ability to inhibit both the activation and function of osteoclasts. Notably, our study extends these prior findings in several important aspects. First, while Tao et al. [23] emphasized the role of UA in enhancing general autophagy, our work reveals that UA specifically suppresses receptor-mediated mitophagy in osteoclasts, suggesting that UA's effects on autophagy/mitophagy are context-dependent and cell type-specific. Second, Wang et al. [24] reported that UA inhibits osteoclast differentiation via BMP-2 signaling, whereas our study identifies *SIRT3* as an additional critical mediator of UA's anti-osteoclastogenic effects, broadening the mechanistic understanding of UA's action. Furthermore, WB analysis revealed a significant reduction in NFATc1 protein levels, a master transcription factor for osteoclastogenesis, providing molecular evidence that UA interferes with the core differentiation program of osteoclasts.

Previous research has indicated that UA ameliorates *PINK1*-dependent mitophagy and mitochondrial respiration [16], highlighting its notable capacity to modulate mitochondria-related functions. However, it is worth noting that in mammalian cells, mitophagy can be categorized into four principal types: *PINK1*/Parkin RBR E3 ubiquitin protein ligase (*PARKIN*)-mediated mitophagy, receptor-mediated mitophagy, lipid receptor-mediated mitophagy, and piecemeal mitophagy [25]. Among these, the *PINK1*/*PARKIN* pathway primarily governs ubiquitin-dependent mitophagy, whereas receptor-mediated mitophagy is activated in distinct cellular contexts and relies on various autophagy receptors constitutively localized to the outer mitochondrial membrane, including Bnip3 and Nix. Our findings demonstrated that UA influenced the expression of *SIRT3*, a member of the mitochondrial deacetylase family in osteoclasts, and regulates the acetylation level of ATPIF1, thus suppressing receptor-mediated mitophagy in these cells. The *SIRT3* overexpression rescue experiment further confirmed that restoring *SIRT3* levels partially reversed UA's inhibitory effects on osteoclast differentiation and mitophagy, supporting the critical role of *SIRT3* in mediating UA's action, but the regulation of ATPIF1 acetylation is still exploratory evidence, and the specific regulation details need to be further confirmed. However, we acknowledge that the absence of *SIRT3* knockdown or pharmacological inhibition data limits the strength of this conclusion, and future studies employing genetic knockdown or conditional knockout of *SIRT3* are needed to provide more definitive evidence. *SIRT3* governs the activity of numerous mitochondrial metabolic enzymes and is indispens-

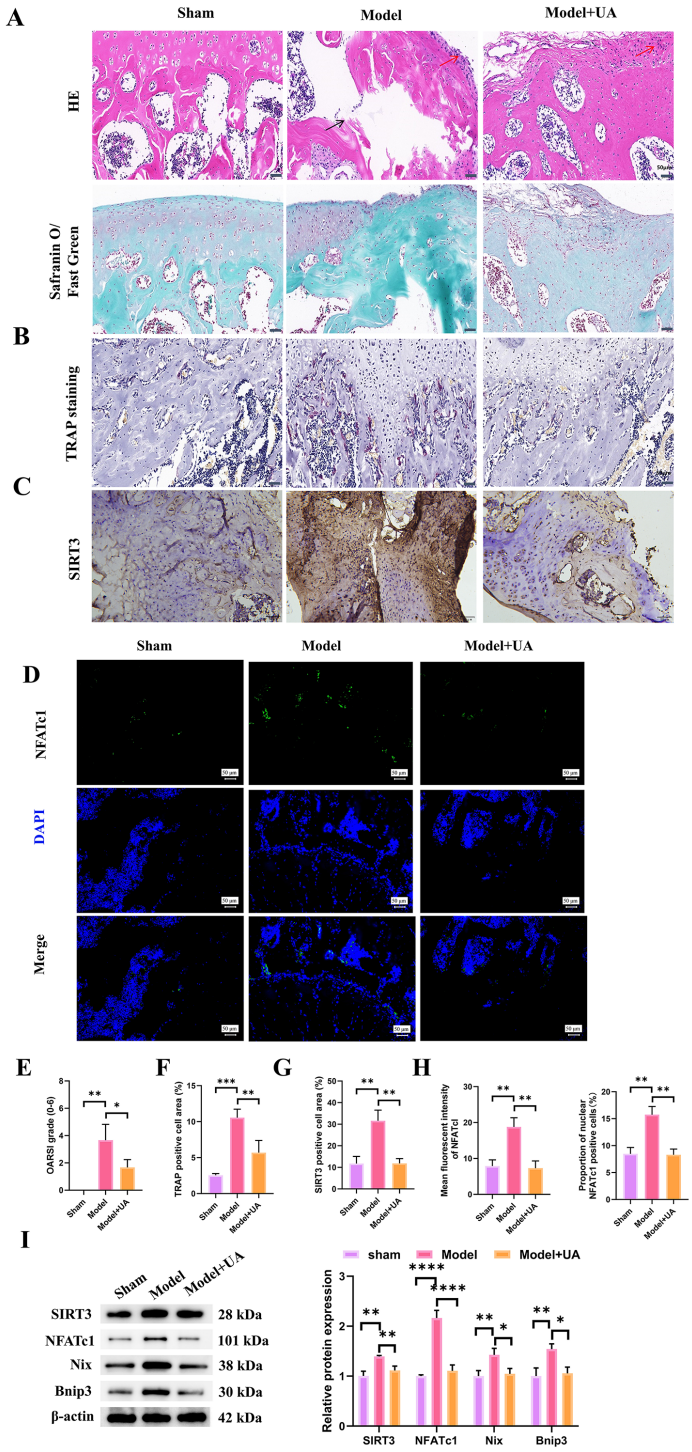

Fig. 3. UA attenuates osteonecrosis. Mice were assigned to Sham, Model, and Model+UA groups. (A,E) Representative H&E and Safranin O/Fast Green staining of mouse femoral tissue sections (A) along with OARSI scores (E) (n = 3); Scale bar was 50 μm. (B,F) TRAP staining of femoral tissue sections (B) and corresponding quantitative analysis (F) (n = 3); Scale bar was 50 μm. (C,G) IHC staining (C) and quantitative analysis (G) of SIRT3 expression in mouse femoral tissues (n = 3); Scale bar was 50 μm. (D,H) IF detection of NFATc1 expression in mouse femoral tissues (D), along with quantitative analysis of its mean fluorescence intensity and nuclear positive cell proportion (H) (n = 3). (I) WB analysis of SIRT3, NFATc1, Nix, and Bnip3 protein levels in the indicated groups (n = 3). *$p < 0.05$, **$p < 0.01$, ***$p < 0.001$, ****$p < 0.0001$. H&E, Hematoxylin and eosin staining; OARSI, Osteoarthritis Research Society International; IHC, Immunohistochemistry; IF, Immunofluorescence.

able for mitochondrial adaptation to diverse stresses [26], and participates in key biological processes including oxidative stress, inflammation, DNA damage, and apoptosis [27]. Meanwhile, *SIRT3* is also a critical driver of aging-related joint disorders such as osteoporosis and osteoarthritis [28,29]. Notably, *SIRT3* is intimately involved in maintaining bone metabolic homeostasis, as its activity is closely linked to osteoclast maturation [9]. Collectively, these findings suggested that UA may influence osteoclast activation by modulating *SIRT3* expression. We also employed a glucocorticoid-induced osteonecrosis mouse model to test UA's impacts on osteonecrosis progression *in vivo*. Results showed that UA treatment not only attenuated cartilage thinning, trabecular collapse, and the disorganized, slender trabeculae in the femoral head, but also reduced SIRT3 protein levels, which indicated that UA mitigated osteonecrosis and highlighted its potential for assessing and monitoring the progression of osteoporosis.

Despite the promising findings, several limitations of this study should be acknowledged. First, while our *SIRT3* overexpression rescue experiments support a critical role for *SIRT3* in mediating the effects of UA on osteoclasts, we acknowledge that the absence of *SIRT3* knockdown (siRNA/shRNA), pharmacological inhibition (e.g., 3-TYP), or osteoclast-specific conditional *SIRT3* knockout models limits the strength of this conclusion. The absence of loss-of-function data indicates that the anti-osteoclastogenic effect of UA can currently only be correlated with *SIRT3* expression, and whether *SIRT3* acts as the sole or predominant mediator responsible for this protective effect remains undetermined. Our conclusions are therefore appropriately tempered to reflect that UA alleviates osteonecrosis "at least in part" through downregulation of *SIRT3*. Future studies employing *SIRT3* knockdown, pharmacological inhibition, and conditional knockout approaches are essential to provide more definitive evidence for the necessity of *SIRT3* in UA's mechanism of action. Second, regarding the mitophagy mechanism, our study demonstrated that UA suppresses receptor-mediated mitophagy markers (Nix and Bnip3) and impairs mitochondrial function in osteoclasts. However, direct visualization of mitophagy flux (e.g., using mitophagy reporter constructs such as mt-Keima or mCherry-GFP-LC3 tandem fluorescence) and rescue experiments with mitophagy inducers were not performed, which would further strengthen the evidence for the mitophagy-dependent mechanism. The current evidence, while consistent with the proposed mechanism, remains indirect and would benefit from these additional validations. Third, our experiments were conducted primarily using mouse-derived bone marrow macrophages and a murine model of glucocorticoid-associated osteonecrosis. The use of female mice for *in vitro* BMMs isolation is a standard practice in the field, enabling the acquisition of sufficient numbers of macrophages with uniform differentiation capacity. The use of male mice for the *in vivo* osteonecrosis model avoids potential interference of estrogen fluctuations during the estrous cycle on bone metabolism and model establishment, thereby ensuring the stability of experimental conditions. Both sets of experiments included strictly matched within-sex internal controls, ensuring that intergroup comparisons were not confounded by sex-related factors. Nevertheless, we acknowledge that species differences may, to some extent, limit the direct extrapolation of our findings to human pathology. Therefore, the applicability of UA in human-derived cells and clinical specimens requires further validation. Fourth, this study focuses predominantly on osteoclasts and receptor-mediated mitophagy within these cells. However, the pathogenesis of osteonecrosis involves multiple cell types, including osteoblasts, vascular endothelial cells, and components of the immune microenvironment, as well as complex intercellular interactions. Whether UA exerts synergistic effects by modulating other cell populations or signaling pathways remains an open question. These limitations highlight the need for further investigations using more complex and multidimensional experimental systems to refine and extend our current findings, which represent an important direction for our future research efforts.

Conclusion

In conclusion, our study demonstrates that UA alleviates osteonecrosis and inhibits osteoclast activation and function, and these beneficial effects are associated with the downregulation of *SIRT3* expression, elevated ATPIF1 acetylation, and the repression of receptor-mediated mitophagy in osteoclasts. These findings provide novel insights into the therapeutic potential of UA for osteonecrosis and bone loss-related diseases.

Availability of Data and Materials

The data used or analyzed during the current study are available from the corresponding author upon reasonable request.

Author Contributions

YX, DHF, PY and XMX contributed to conceptualization, methodology, and drafting the manuscript. TL, YFG, and JLZ contributed to data curation, formal analysis and revising the manuscript critically for important intellectual content. All authors gave final approval of the version to be published. All authors have participated sufficiently in the work to take public responsibility for appropriate portions of the content and agreed to be accountable for all aspects of the work in ensuring that questions related to its accuracy or integrity.

Ethics Approval and Consent to Participate

All animal procedures were approved by the Animal Research Ethics Committee of Changshu Hospital Affiliated to Nanjing University of Chinese Medicine (approval date: September 5, 2025), and conducted in strict accordance with the Guide for the Care and Use of Laboratory Animals (8th ed., National Academies Press, 2011) and the ARRIVE Guidelines 2.0.

Acknowledgment

Not applicable.

Funding

This study was supported by 2021 Changshu Municipal Health Commission Science and Technology Plan Key Funded Project (Grant No. CSWS202105).

Conflict of Interest

The authors declare no conflict of interest.

References

[1] George G, Lane JM. Osteonecrosis of the Femoral Head. Journal of the American Academy of Orthopaedic Surgeons. Global Research & Reviews. 2022; 6: e21.00176. https://doi.org/10.5435/JAAOSGlobal-D-21-00176

[2] Zhang J, Cao J, Liu Y, Zhao H. Advances in the Pathogenesis of Steroid-Associated Osteonecrosis of the Femoral Head. Biomolecules. 2024; 14: 667. https://doi.org/10.3390/biom14060667

[3] Karampinas P, Galanis A, Papagrigorakis E, Vavourakis M, Vlachos C, Zachariou D, et al. Osteonecrosis of the Femoral Head. Optimizing the Early-Stage Joint-Preserving Surgical Treatment? Maedica. 2022; 17: 948–954. https://doi.org/10.26574/maedica.2022.17.4.948

[4] Kobayashi S, Sugano N, Ando W, Fukushima W, Kondo K, Sakai T. Factors associated with dislocation after total hip arthroplasties performed for nontraumatic osteonecrosis of the femoral head: a multicenter cohort study of 5,983 hips. Acta Orthopaedica. 2025; 96: 348–355. https://doi.org/10.2340/17453674.2025.43473

[5] Chen K, Liu Y, He J, Pavlos N, Wang C, Kenny J, et al. Steroid-induced osteonecrosis of the femoral head reveals enhanced reactive oxygen species and hyperactive osteoclasts. International Journal of Biological Sciences. 2020; 16: 1888–1900. https://doi.org/10.7150/ijbs.40917

[6] Juszczak F, Arnould T, Declèves AE. The Role of Mitochondrial Sirtuins (SIRT3, SIRT4 and SIRT5) in Renal Cell Metabolism: Implication for Kidney Diseases. International Journal of Molecular Sciences. 2024; 25: 6936. https://doi.org/10.3390/ijms25136936

[7] Ji Z, Liu GH, Qu J. Mitochondrial sirtuins, metabolism, and aging. Journal of Genetics and Genomics = Yi Chuan Xue Bao. 2022; 49: 287–298. https://doi.org/10.1016/j.jgg.2021.11.005

[8] Zhang T, Wang L, Duan X, Niu Y, Li M, Yun L, et al. Sirtuins mediate mitochondrial quality control mechanisms: a novel therapeutic target for osteoporosis. Frontiers in Endocrinology. 2024; 14: 1281213. https://doi.org/10.3389/fendo.2023.1281213

[9] Richardson KK, Adam GO, Ling W, Warren A, Marques-Carvalho A, Thostenson JD, et al. Mitochondrial protein deacetylation by SIRT3 in osteoclasts promotes bone resorption with aging in female mice. Molecular Metabolism. 2024; 88: 102012. https://doi.org/10.1016/j.molmet.2024.102012

[10] Li N, Li X, Zheng K, Bai J, Zhang W, Sun H, et al. Inhibition of Sirtuin 3 prevents titanium particle-induced bone resorption and osteoclastsogenesis via suppressing ERK and JNK signaling. International Journal of Biological Sciences. 2021; 17: 1382–1394. https://doi.org/10.7150/ijbs.53992

[11] Liu X, Diao L, Zhang Y, Yang X, Zhou J, Mao Y, et al. Piperlongumine Inhibits Titanium Particles-Induced Osteolysis, Osteoclast Formation, and RANKL-Induced Signaling Pathways. International Journal of Molecular Sciences. 2022; 23: 2868. https://doi.org/10.3390/ijms23052868

[12] D'Amico D, Andreux PA, Valdés P, Singh A, Rinsch C, Auwerx J. Impact of the Natural Compound Urolithin A on Health, Disease, and Aging. Trends in Molecular Medicine. 2021; 27: 687–699. https://doi.org/10.1016/j.molmed.2021.04.009

[13] Rogovskii VS. The Therapeutic Potential of Urolithin A for Cancer Treatment and Prevention. Current Cancer Drug Targets. 2022; 22: 717–724. https://doi.org/10.2174/1568009622666220602125343

[14] Wojciechowska O, Kujawska M. Urolithin A in Health and Diseases: Prospects for Parkinson's Disease Management. Antioxidants (Basel, Switzerland). 2023; 12: 1479. https://doi.org/10.3390/antiox12071479

[15] Gao Z, Yi W, Tang J, Sun Y, Huang J, Lan T, et al. Urolithin A protects against acetaminophen-induced liver injury in mice via sustained activation of Nrf2. International Journal of Biological Sciences. 2022; 18: 2146–2162. https://doi.org/10.7150/ijbs.69116

[16] D'Amico D, Olmer M, Fouassier AM, Valdés P, Andreux PA, Rinsch C, et al. Urolithin A improves mitochondrial health, reduces cartilage degeneration, and alleviates pain in osteoarthritis. Aging Cell. 2022; 21: e13662. https://doi.org/10.1111/acel.13662

[17] Tao H, Li W, Zhang W, Yang C, Zhang C, Liang X, et al. Urolithin A suppresses RANKL-induced osteoclastogenesis and postmenopausal osteoporosis by, suppresses inflammation and downstream NF-κB activated pyroptosis pathways. Pharmacological Research. 2021; 174: 105967. https://doi.org/10.1016/j.phrs.2021.105967

[18] Ghosh N, Das A, Biswas N, Gnyawali S, Singh K, Gorain M, et al. Urolithin A augments angiogenic pathways in skeletal muscle by bolstering NAD^+ and SIRT1. Scientific Reports. 2020; 10: 20184. https://doi.org/10.1038/s41598-020-76564-7

[19] Severmann AC, Jochmann K, Feller K, Bachvarova V, Piombo V, Stange R, et al. An altered heparan sulfate structure in the articular cartilage protects against osteoarthritis. Osteoarthritis and Cartilage. 2020; 28: 977–987. https://doi.org/10.1016/j.joca.2020.04.002

[20] Hubert J, Hawellek T, Moe M, Hischke S, Krause M, Rolvien T, et al. Labral calcification in end-stage osteoarthritis of the hip correlates with pain and clinical function. Journal of Orthopaedic Research : Official Publication of the Orthopaedic Research Society. 2018; 36: 1248–1255. https://doi.org/10.1002/jor.23736

[21] Shoji T, Shozen H, Ueki S, Kaneta H, Yaunaga Y, Adachi N. Evaluation of the long-term patient-reported outcomes after hip arthroplasty or joint preserving with Sugioka femoral osteotomy in patients with femoral head osteonecrosis. International Orthopaedics. 2024; 48: 1201–1208. https://doi.org/10.1007/s00264-024-06118-3

[22] Yang H, Nie S, Zhou C, Li M, Yu Q, Mo Y, et al. Palliative effect of rotating magnetic field on glucocorticoid-induced osteonecro-

sis of the femoral head in rats by regulating osteoblast differentiation. Biochemical and Biophysical Research Communications. 2024; 725: 150265. https://doi.org/10.1016/j.bbrc.2024.150265

[23] Tao H, Tao Y, Yang C, Li W, Zhang W, Li X, et al. Gut Metabolite Urolithin A Inhibits Osteoclastogenesis and Senile Osteoporosis by Enhancing the Autophagy Capacity of Bone Marrow Macrophages. Frontiers in Pharmacology. 2022; 13: 875611. https://doi.org/10.3389/fphar.2022.875611

[24] Wang Z, Qi G, Li Z, Cui X, Guo S, Zhang Y, et al. Effects of urolithin A on osteoclast differentiation induced by receptor activator of nuclear factor-κB ligand via bone morphogenic protein 2. Bioengineered. 2022; 13: 5064–5078. https://doi.org/10.1080/21655979.2022.2036893

[25] Uoselis L, Nguyen TN, Lazarou M. Mitochondrial degradation: Mitophagy and beyond. Molecular Cell. 2023; 83: 3404–3420. https://doi.org/10.1016/j.molcel.2023.08.021

[26] Wang T, Cao Y, Zheng Q, Tu J, Zhou W, He J, et al. SENP1-Sirt3 Signaling Controls Mitochondrial Protein Acetylation and Metabolism. Molecular Cell. 2019; 75: 823–834.e5. https://doi.org/10.1016/j.molcel.2019.06.008

[27] Ning Y, Dou X, Wang Z, Shi K, Wang Z, Ding C, et al. SIRT3: A potential therapeutic target for liver fibrosis. Pharmacology & Therapeutics. 2024; 257: 108639. https://doi.org/10.1016/j.pharmthera.2024.108639

[28] Hu S, Wang S. The Role of SIRT3 in the Osteoporosis. Frontiers in Endocrinology. 2022; 13: 893678. https://doi.org/10.3389/fendo.2022.893678

[29] Zhang Y, Liu Y, Hou M, Xia X, Liu J, Xu Y, et al. Reprogramming of Mitochondrial Respiratory Chain Complex by Targeting SIRT3-COX4I2 Axis Attenuates Osteoarthritis Progression. Advanced Science (Weinheim, Baden-Wurttemberg, Germany). 2023; 10: e2206144. https://doi.org/10.1002/advs.202206144